Excited State Dynamics and Structures of Functionalized Phthalocyanines. 1. Self-Regulated Assembly of Zinc Helicenocyanine

Lin X. Chen,*,† George B. Shaw,† David M. Tiede,† Xiaobing Zuo,† Peter Zapol,†,‡ Paul C. Redfern,† Larry A. Curtiss,†,‡ Thanasat Sooksimuang,§ and Braja K. Mandal§

Chemistry Division and Materials Science Division, Argonne National Laboratory, Argonne, Illinois 60439, and Department of Biological, Chemical and Physical Sciences, Illinois Institute of Technology, Chicago, Illinois 60616

Received: April 14, 2005; In Final Form: June 27, 2005

Recently synthesized zinc helicenocyanine (ZnHc), where four helicene groups are fused with a phthalocyanine (Pc) core through all-carbon linkages, exhibits an unusually strong tendency of forming soluble molecular aggregates in organic solvents. The aggregation results in a strong optical absorption across most of the visible region, which is drastically different from that of its monomer. The aggregation is suppressed by dissolving ZnHc in a liquid crystal, octylbiphenylcarbonitrile (OBCN), where the monomer ZnHc dominates and exhibits a typical optical absorption spectrum of monomeric zinc phthalocyanine, except red shift in both Q- and B- bands due to π-conjugation expansion. This study correlates optical properties and excited state dynamics of ZnHc with intra- and intermolecular electronic interactions, using quantum mechanical calculations and ultrafast transient absorption spectroscopy. Structural details of the aggregates are revealed by small-angle X-ray scattering (SAXS) to be uniformly dimers with alkoxy chains wrapped around the core of a face-to-face dimer. The results suggest that while the peripheral helicene moieties in ZnHc are electronically coupled to the Pc core via expansion of the π-conjugation of the macrocycle, the coupling is attenuated by the "lock washer" conformation of the nonplanar peripheral helicenes which prevents π-conjugation throughout the entire macrocycle. The interplay between π-conjugation expansion in the macrocyle plane and the $\pi-\pi$ stacking out of the macrocyle plane produces a structure that facilitates the unique optical properties and self-regulated assembly into nanoscale structures in solution. These novel optical properties are explored for potential applications in various areas.

Introduction

Phthalocyanines (Pcs) have been studied extensively because of their applications in photonics,[1−3] data storage,[4] photocatalysis,[5−8] photodynamic therapy,[9,10] and solar energy conversion.[11,12] Optical properties of Pcs can be controlled and manipulated through binding different metal ions with various axial ligands, and covalently attaching different side groups.[13−15] In particular, Pcs self-assemble into nanometer scaled aggregates via nonbonding interactions, such as π-stacking, in films, liquid crystals, and solutions, and such stacking can be controlled via chemical modifications.[16−22] One of the approaches of controlling self-assembly is through steric hindrance of peripheral groups which prevent the π-stacking. Hence, the self-assembly of Pcs can be regulated by these two structural factors exerting two opposite effects. We report here the first in a series of studies on helicene fused Pcs, helicenocyanine (Hc) (Figure 1). Helicenes have chiral aromatic structures with spiral arrangements and can self-assemble into nanoscale spiral structures with unique optical properties.[23−25] When helicenes are fused with phthalocyanine, the unique optical and chemical properties occur due to the interplay of the electronic properties between these groups. These properties are explored here.

The helicenes fused with the Pc core to form Hc have a curved pentacene structure, where the middle benzyl ring is

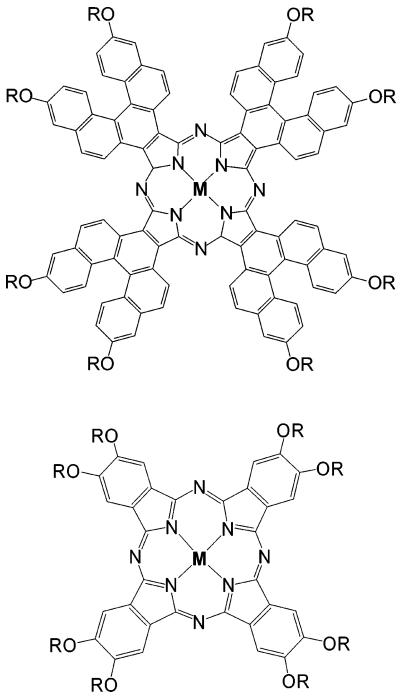

Figure 1. Top: ZnHc, tetrakis-β-4,9,19,24,34,39,49,54-octadodecyloxy helicenocyanine (M = Zn or 2H, R=$C_{12}H_{25}$). Bottom: ZnPc, tetrakis-β-4,9,19,24,34,39,49,54-octadodecyloxy phthalocyanine (M = Zn or 2H, R=$C_{12}H_{25}$).

† Chemistry Division, Argonne National Laboratory.
‡ Materials Science Division, Argonne National Laboratory.
§ Illinois Institute of Technology.

10.1021/jp051947w CCC: $30.25
Published on Web 08/17/2005

shared with the Pc core to form an extended π-conjugated macrocycle (Figure 1). The octadodecyloxy chains are attached to the ends of the helicene. Although Hc has a larger aromatic macrocycle than Pc, its nonplanar conformation prevents the π-conjugation throughout the entire molecule. We discovered an unusually strong self-assembly of zinc coordinated Hc, ZnHc, in solution at room temperature, as well as unique optical properties in its molecular aggregates. The combination of peripheral helicenes of ZnHc promotes self-assembly, while strong van der Waals interactions between Pc cores facilitate unique conformation of the helicene groups in the molecular aggregates. To understand the interplay between different chromophores fused into a presumed π-conjugated macrocyclic system, we investigated intramolecular electronic couplings between helicenes and Pc core, as well as intermolecular interactions in self-assembled ZnHc aggregates in terms of structural origins of their unique optical properties. These results should lead to future exploration of controlled self-assembly for nanoscale molecular materials in various applications.

Experimental and Computational Methods

Synthesis and Samples. Zinc tetrakis-β-4,9,19,24,34,39,49,-54-octadodecyloxy helicenocyanine (ZnHc) was synthesized according to the methodology reported for its unsubstituted precursor.[26] The synthesis of ZnHc started with the preparation of a new diene, 6,6′-dimethoxy-3,3′,4,4′-tetrahydro-1,1′-dinaphthyl, by pinacolization of 6-methoxy-1-tetralone followed by dehydration of the pinacol. The Diels−Alder reaction of the diene with a large excess of fumaronitrile gave a dinitrile adduct, which on treatment with *N*-bromosuccinimide, followed by dehydrobromination using sodium acetate provided fully aromatized dimethoxy dinitrile monomer. The attachment of dodecyl groups to the monomer was performed at this stage by demethylation followed by O-alkylation. ZnHc was obtained by cyclic tetramerization of the monomer in the presence of a hindered base and zinc chloride. ZnHc was found to be readily soluble in common organic solvents such as THF, toluene, and chloroform. The details synthesis of ZnHc can be found elsewhere.[26] Zinc tetrakis-β-4,9,19,24,34,39,49,54-octadodecyloxy phthalocyanine (ZnPc) and the liquid crystal octylbiphenylcarbonitrile (OBCN) were purchased from Aldrich Chemicals and used without further purification.

Steady-State and Ultrafast Transient Optical Spectroscopy. Steady-state optical absorption spectra were measured using a Shimadzu UV−visible spectrophotometer (UV-1601). Emission and excitation spectra were obtained with a Photon Technology International fluorimeter. ZnHc with 5×10^{-6} M toluene solution in a 2-mm path quartz cuvette or with 10^{-3} to 10^{-4} M liquid crystal solutions sandwiched between two microscope slides were used for the absorption and fluorescence measurements, respectively.

Ultrafast transient absorption (TA) spectral and kinetics were measured by an amplified Ti:sapphire laser system with an optical parametric amplifier (OPA) as described elsewhere.[27] Excitation laser pulses were derived from either the second harmonic of the Ti:Sapphire regenerative amplifier at 410 nm, or the output of the OPA tunable from 470 to 800 nm. White light continuum probe pulses were generated by focusing a few μJ of the Ti:sapphire amplifier output onto a sapphire disk. The resulting probe beam was split into the reference and the measuring beams. The white light probe beam and the 200-nJ pump beam were focused to a 0.3-mm diameter spot at the sample with a nearly collinear geometry. The optical density of the sample was kept below 0.3 at 410 nm, and the sample cuvette was 2-mm thick. The pump and probe pulses were about 90 fs fwhm, and the instrumental response function was 180 fs fwhm.

Small-Angle X-Ray Scattering. Small-angle X-ray scattering (SAXS) measurements were carried out at the undulator beamline 12-ID at the Advanced Photon Source (APS), Argonne National Laboratory, utilizing a double-crystal Si(111) monochromator and a MarCCD detector.[28] The X-ray wavelength was set at $\lambda = 1.0$ Å, and the sample to detector distance was adjusted to achieve scattering measured across the range of momentum transfer $0.02\ \text{Å}^{-1} < q < 0.8\ \text{Å}^{-1}$, where $q = (4\pi/\lambda)\sin\theta$, and λ is the X-ray wavelength and 2θ is the scattering angle. Precautions to prevent radiation damage to the sample include the use of a flow cell and short exposure times of 20 s per image.[29] Data from 10 images were averaged. Calculations and curve fitting were performed with Origin 7.0 (Microcal Software, Inc., Northampton, MA). The *P*(r) distance distribution function (PDDF) was calculated from the scattering data using the program GNOM.[30] Model-independent structures for ZnHc aggregate were calculated from solution SAXS data with programs DAMMIN[31] and GNOM.[30]

Quantum Mechanical Computation. The structures of ZnPc and ZnHc monomers were optimized at various levels of theory including PM3,[32,33] HF/STO-3G*,[34] HF/MINI1* [*refers to a p-type polarization function (0.095) on Zn],[35] HF/3-21G,[34] HF/6-31G*,[34] B3LYP/3-21G, and B3LYP/6-31G*. The B3LYP[36] density functional method gives the best agreement with the experimental structure of ZnPc,[37] although HF/MINI1* does reasonably well and is used for the dimer and trimer structures. Molecular scale factors[38] were used on H, C, N, and O atoms for MINI1* calculations because this improved the agreement between theoretical and experimental geometries of ZnPc.

Stacking interactions were investigated by calculating interaction energies of dimers and trimers at the HF/MINI1* level of theory. Frozen geometries (HF/MINI1*) were used for the monomers. Dispersion energy, which is not included at the Hartree−Fock level, was calculated using the London dispersion formula

$$E^{\mathrm{D}} = \sum_{\alpha=1}^{M_1}\sum_{\beta=1}^{M_1}\frac{3}{2}\left[\frac{I_\alpha I_\beta P_\alpha P_\beta}{(I_\alpha + I_\beta)R_{\alpha\beta}^{\ 6}}\right] \tag{1}$$

where I_α is the ionization potential and P_α is the polarizability of atom α, the summations over α and β are carried out over all atoms in the monomers M_1 and M_2, and $R_{\alpha\beta}$ is the distance between atoms α and β. The valence state atomic polarizabilities and ionization potentials are used.[39] Since the London formula is only valid for the interaction of two systems with nonoverlapping densities, a damping function was used at small distances.[40] The damping function $f(R_{\alpha\beta})$ multiplies each term in eq 1 and has the has the following form:

$$f(R_{\alpha\beta}) = \left[1 - \exp\left(-3\cdot\left(\frac{R_{\alpha\beta}}{R_{\mathrm{o}}}\right)^7\right)\right]^4 \tag{2}$$

The R_{o} value used was 3.1856 Å. This value was derived for a Zn_2 and was used for all of the other atoms since the Zn has a van der Waals radius of 1.4 Å, which is similar to those of first row atoms (e.g., oxygen = 1.5 Å, also hydrogen = 1.2−1.45 Å). This R_{o} value along with the atomic polarizability (7.2203 Å^3) and ionization potential (9.6736 eV) of zinc were obtained by fitting the Zn dimer (damping function)*(dispersion) energies to (MP2−HF) correlation energies at several Zn Zn distances between 3 and 5 Å using the G3MP2Large basis set.[41]

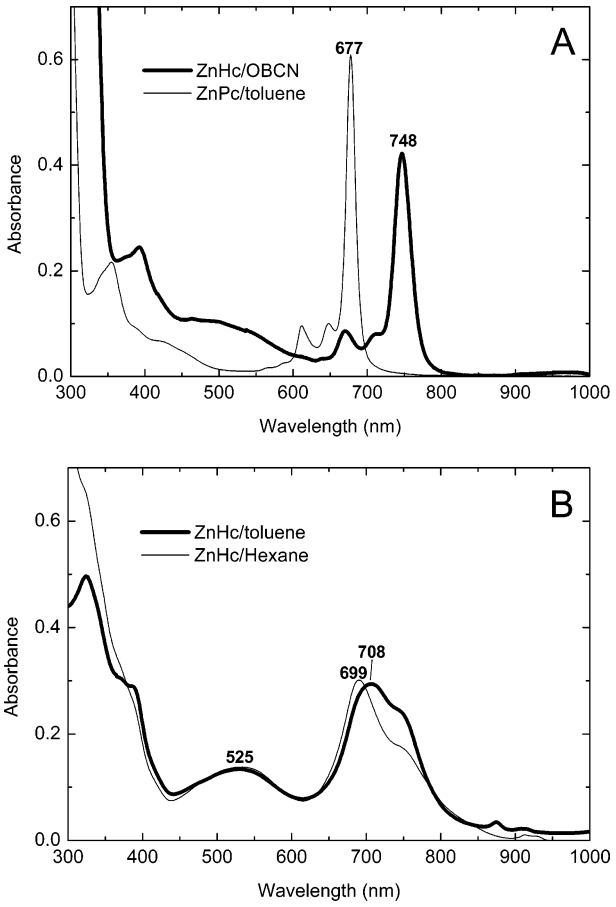

Figure 2. (A) Monomeric absorption spectra of ZnHc in liquid crystal OBCN, along with absorption spectra of ZnPc in toluene. ZnHc in OBCN was measured by sandwiching a thin liquid crystal film (a few micrometers thick, about 4×10^{-5} M) between two microscope slides, and the absorbance was enlarged by a factor of 10. (B) Aggregate absorption spectra of ZnHc solution was measured in a 2-mm path cuvette with a concentration of about 5×10^{-6} M.

The results from eqs 1 and 2 are in reasonable agreement with MP2/6-31G* calculations performed on ZnHc dimer, which explicitly include some dispersion energy, but are prohibitively expensive for the large systems in this study. The MP2/6-31G* calculations were done on the ZnHc dimer with monomers frozen at the B3LYP/6-31G* optimized geometries.

Using the ArgusLab 3.2. program, ZINDO/S [42,43] calculations were performed for helicene, ZnPc, ZnHc monomer, dimer and trimer. All configuration interaction calculations involved a window of 30 occupied and 30 unoccupied molecular orbitals. Molecular geometries that were previously optimized at various levels of theory (PM3, HF/MINI-1, HF/3-21G, B3LYP/3-21G, B3LYP/6-31G*) were used to analyze the sensitivity of the optical spectra to the level of approximation for structural optimization.

Results

Steady-State Absorption and Emission. Figure 2A,B shows absorption spectra of ZnHc in liquid crystal OBCN and in toluene. The former has a sharp Q-band with a typical shape for the Pc monomers,[44] whereas the latter has a typical shape for the Pc aggregates with a broadened and blue-shifted main peak from its monomer Q-band.[45,46] Comparing ZnHc and ZnPc in toluene at the same concentration (i.e., 5×10^{-6} M), the Q-band of ZnHc significantly broadens and blue-shifts relative to its monomer band, while the Q-band of ZnPc still maintains the same shape as the monomer band. Similar shapes of the broadened Q-band for ZnHc are also observed in several other solvents, though the shape and the energy of the broadened Q-band vary, as illustrated in Figure 2B using hexane as an example. The broadened Q-band of ZnHc in toluene remains even at a concentration as low as 10^{-7} M, suggesting its extraordinary tendency of forming soluble aggregates. In contrast, the Q-band of ZnPc in toluene only slightly broadens at 10^{-4} M and does not have a distinctive blue shift. The blue-shifted Q-band from 748 to 708 nm for ZnHc in toluene solution is an indication of the H-aggregate formation where only the transition from the ground state to the upper exciton state is allowed.[45,46] However, a weak absorption "tail" on the red side of the monomer Q-band of ZnHc indicates possible contribution of J-aggregates due to slight sliding between adjacent stacked monomers. The blue-shift for the B-band, however, is significantly smaller that for the Q-band as shown in Figure 2.

The Q-band of ZnHc at 748 nm in OBCN appears to have the same shape as that for monomeric ZnPc at 677 nm, indicating the existence of mostly monomers (Figure 2A), although it is red-shifted by 1402 cm^{-1} due to the expansion of the π-conjugation by four additional aromatic rings fused on each benzyl ring of the Pc. However, the red-shift is still smaller than that for ZnNc (2,3-Nc, naphthalocyanine) from ZnPc,[47a] but is larger than that for ZnNc (1,2-Nc with all identical conformers).[47b] The Q-band at 748 nm for monomeric ZnHc is still lower in energy than the Q-band at 726 nm for a ZnPc fused with larger helicene groups coupled through N-atoms in a previous study.[48] These observations demonstrate that the nonplanar helicene prevents the π-conjugation throughout the entire ZnHc, while the C-atom coupling between the Pc core and the peripheral helicene groups facilitates a stronger π-conjugation than the N-atom counterpart. The width of the Q-band, 466 cm^{-1}, for monomeric ZnHc is broader than that of 326 cm^{-1} for ZnPc, which is likely due to nonuniform chiral conformations of the helicene groups that could slightly alter transition dipoles for each individual molecule. Meanwhile, the red shift of 2528 cm^{-1} is also observed for the B-band at 390 nm for ZnHc from that at 355 nm for ZnPc. The red shift is even observed for a very broad and weak absorption with a shoulder feature in 450−600 nm region for monomeric ZnHc from that in 400−500 nm region for ZnPc. This shoulder feature was attributed to an n-π* transition in alkoxy substituted phthalocyanines.[49,50] Interestingly, this shoulder feature becomes a pronounced absorption band centered at 525 nm in the absorption spectrum of ZnHc in toluene, which was not commonly observed except for charge-transfer species of open-shell transition metallophthalocyanines,[51,52] metallophthalocyanine cations (i.e., $ZnPc^+$),[53] and Pc films.[54] The intensity of this broad 525 nm band increases concurrently with the blue-shifted and broadened Q-band for ZnHc in solution as seen in Figure 2B.

The emission spectrum of monomeric ZnHc in OBCN (Figure 3A) has a peak at 756 nm with a near mirror image of the monomeric Q-band and a very small Stoke-shift. A weaker blue fluorescence peak around 425 nm is also observed and is assigned as the fluorescence from the upper excited-state S_2.[55,56] The excitation spectrum of ZnHc in OBCN monitored at 759 nm emission peak resembles the ground-state absorption spectrum of the monomer (not shown).

In contrast, a broad emission peak of self-assembled ZnHc in toluene appears at 510 nm while the expected emission from the lowest excited-state S_1 is severely quenched (Figure 3B) as observed in other Pc aggregates.[45,57,58] Such a quenching of

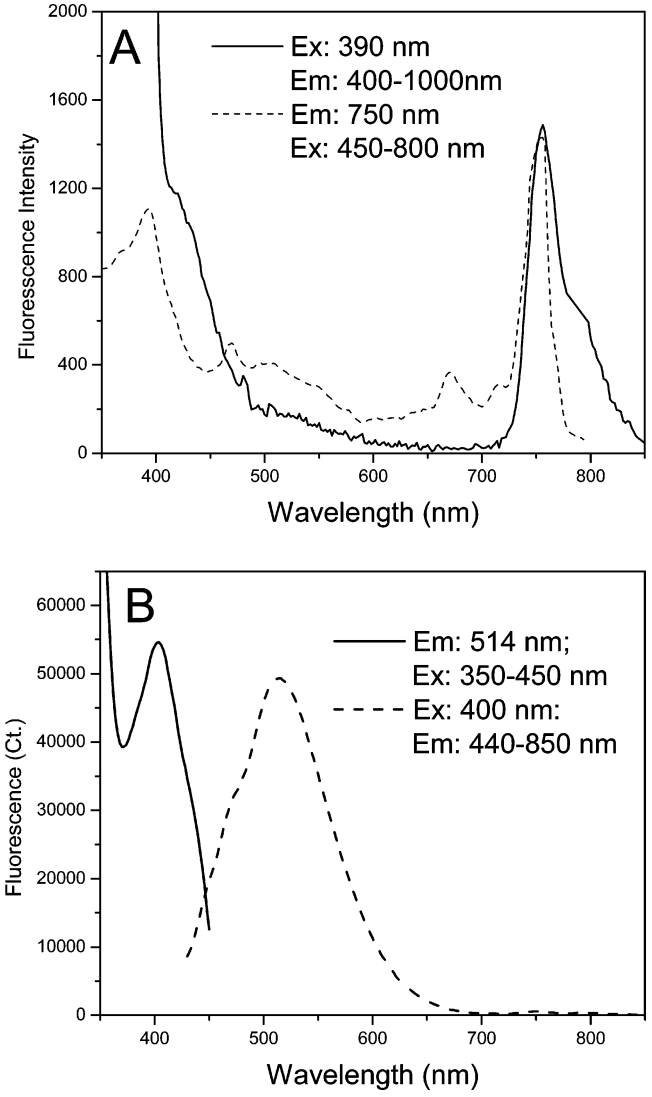

Figure 3. Emission and excitation spectra of ZnHc in (A) OBCN liquid crystal and in (B) toluene.

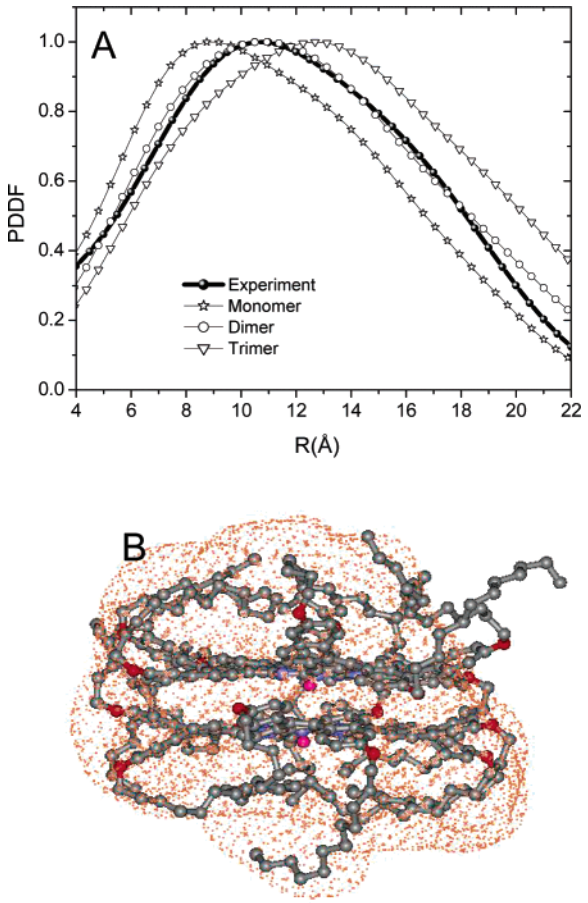

Figure 4. (A) Pair distance distribution functions (PDDF) from experimental scattering data and calculated patterns using Gnom program. The PDDF functions are normalized at the peak to illustrate the relative shifts; (B) a model-independent shape (in dot clouds) for ZnHc shown above was obtained with DAMMIN in Jagged mode and manually superimposed unto a structure after the MD simulation (see text).

fluorescence has been attributed to the internal conversion from upper to lower exciton states followed by nonradiative decay to the ground state.[46] The 510 nm emission peak resembles that in self-assembled helicene observed in a previous study,[59] so its origin may be related to $\pi-\pi$ interactions between helicene moieties in ZnHc aggregates, which will be discussed in detail. The excitation spectrum monitored at 510 nm emission reveals a peak at 402 nm, red-shifted from the B-band at 390 nm in toluene. We have carefully ruled out the possibility of any impurity by the same measurement in blank toluene. This emission is absent in ZnHc dissolved in OBCN and in blank toluene. Hence, the excitation peak at 402 nm is one of the intrinsic properties of self-assembled ZnHc in toluene.

Structure of Self-Assembled ZnHc in Solution. While the broadened Q-band in the ground-state absorptionspectrum of ZnHc in toluene (Figure 2) is indicative of its strong tendency of aggregation, it offers little insight into direct structural details of the aggregates. Using small-angle X-ray scattering (SAXS) in conjunction, the size and shape of ZnHc aggregates can be investigated.

The Guinier plot (shown in supplemental information) of ZnHc aggregates in toluene fits well to a linear function with an average radius of gyration $R_g = 7.95 \pm 0.05$ Å, indicating a uniform size distribution. Nevertheless, calculated scattering patterns for monomeric or dimeric ZnHc with all-trans extended octa-dodecyloxy chains result in R_g values almost twice that of the experimental value. Hence, this conformation with all-trans octa-dodecyloxy chains is unlikely the structure of ZnHc in solution. This assessment is supported by calculations that combine the energy minimization with MM+ force field and the molecular dynamics (MD) simulation (Hyperchem, Hypercube). The starting structures of the dimer for energy minimization have two monomers separated by 3−5 Å between macrocycles, with either 0° or 45° rotation in the Pc plane relative to each other, and with all-trans extended octadodecyloxy chains. The resulting structure after the energy minimization from different starting structures is converged to a face-to-face stacked dimeric ZnHc with Zn−Zn distance of 3.6 Å, relative in-plane rotation angle of about 15−20° and nearly perfectly extended octadodecyloxy chains of all-trans conformation. This structure is then undergone MD simulation at 293K for several hundred picoseconds. The initially all-trans extended octa-dodecyloxy chains of ZnHc and its face-to-face dimer evolve into random coils wrapped around the stacked Pcs with an energy 130 kcal/mol lower than the one with all-trans extended octadodecyloxy chains. Parallel calculations are also performed on a stacked ZnHc trimer. The contour of the resulting ZnHc dimer overlays with that of a cluster generated by a model-independent DAMMIN calculation based on the experimental data (Figure 4B), whereas the agreements for monomer and trimer are poor. The preferred agreement for the dimeric aggregates is demon-

strated by the pair density distribution function (PDDF) (Figure 4A).

In principle, there are six different isomers of ZnHc monomer, which differ by the two possible orientations of the helices (denoted here **1** and **2**) in each of the four helicene moieties, **1111**, **2222**, **1112**, **2221**, **1122**, and **1212** with degeneracies of 1, 1, 4, 4, 4, and 2. Quantum mechanical calculations at the B3LYP/6-31G*//HF/MINI1* level indicate that there is an energy difference of 9.12 kcal/mol between the most stable isomer with four identically oriented helicene moieties (**1111**, or its isoenergetic mirror image **2222**) and an isomer with two opposing helicene ligands reflected in the core plane (**1212**). This is the result of steric hindrance between the adjacent helicene groups, which gives an energy penalty of 4.56 kcal/mol for flipping each helicene relative to its neighbors. Taking into account degeneracies of the isomers and calculated energy differences between them, we have obtained the distribution of the isomers at room temperature from the electronic part of the partition function. The resulting distribution is dominated by **1111** and **2222** isomers, together giving 99.7% of the total number of ZnHc monomers. Thus, only these two isomers were considered in the models of the dimers. The two dimer models contain either face-to-face identical monomers or two mirror image isomers. The distance between the dimers and the relative rotation angle around the Zn−Zn axis were allowed to change. The structures of ZnHc dimers with frozen monomers were also optimized using HF/MINI1(*) and dispersion correction. Two stable dimers were found, **1111/1111** or **2222/2222** and **1111/2222**, where monomers are rotated by 22.5° and 45° relative to each other (with mirror image isomers), respectively. The second configuration **1111/2222** is about 20 kcal/mol more stable than the first with interaction energy of 64.2 kcal/mol (attractive). In this geometry, the Zn−Zn distance is 3.95 Å. This is somewhat higher than the MM+ result, due to geometry restrictions in the ab initio study and difference in methodology. We have also performed ZINDO/S calculations on ZnHc dimer geometry obtained from MM+ molecular dynamics simulations. The results (not shown) are in qualitative agreement with those from ab initio geometries, except small splitting of the peaks due to the asymmetry of the monomers in the course of the simulation.

Ultrafast Excited-State Dynamics of ZnHc in Liquid Crystal and in Toluene. Two lowest-energy electronic transitions corresponding to the Q and B bands are due to $\pi-\pi^*$ transitions in porphyrins by Gouterman's four-level model, and are similarly assigned in phthalocyanines by Stillman's calculation.[53] The ground and first two lowest-energy excited singlet states generated via transitions responsible for the Q- and B-bands in zinc phthalocyanines are designated to S_0, S_1, and S_2 states. For the face-to-face dimeric aggregates (H-aggregates) of ZnHc in toluene as suggested in the last section, the exciton splitting of the absorption occurs, and the additional broad absorption band centered at 525 nm appears. To investigate the correlation between excited states and excited state dynamics in ZnHc aggregates, excitation wavelengths of 410, 540 and 690 nm were selected to respectively excite the B-band, the 525 nm broad band, and the Q-band for solution sample. In particular, the origin of the 525 nm broad band and its correlation to other known S_2 and S_1 states is investigated.

ZnHc Monomer in Liquid Crystal. We first examine the TA spectra of monomeric ZnHc in OBCN and the monomeric ZnPc in toluene (Figure 5), which display similar overall shapes of the Q-band ground-state bleaching (GB), but different shapes in the excited-state absorption (EA) in the region below 650 nm. ZnPc monomer in dilute toluene has the GB of the Q-band at 677 nm and the EA peaked at 550 nm, agreeing with previous studies.[46] In contrast, monomeric ZnHc in OBCN has the GB of the Q-band at 748 nm and a flat featureless EA below 650 nm. The absence of the GB centered at 525 nm suggests that this broad band originates from molecular aggregates of ZnHc.

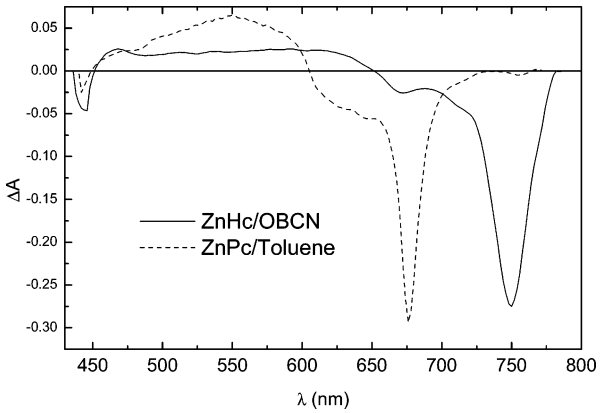

Figure 5. Room-temperature TA spectra at 10 ps after 414 nm excitation for ZnHc in OBCN and ZnPc in toluene.

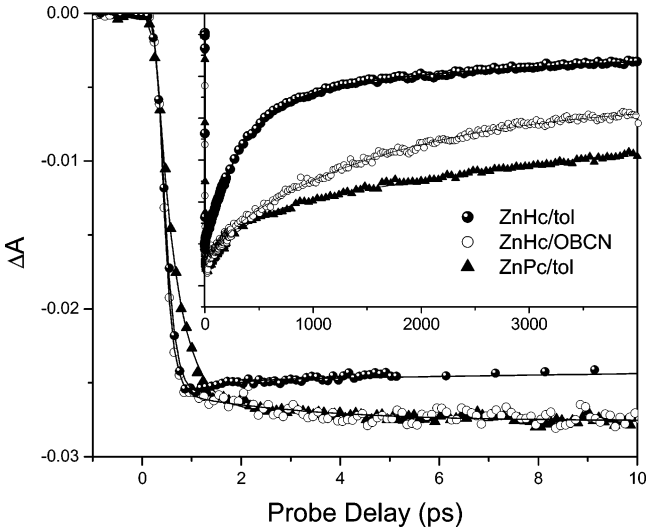

Figure 6. The ground-state recovery kinetics of ZnHc in OBCN measured at 750 nm, and in toluene at 700 nm, along with that of ZnPc in toluene measured at 675 nm. The excitation wavelength is 410 nm.

For monomeric ZnHc in OBCN, the Q-band GB detected at 750 nm can be described by a major (80%) and a minor (20%) components with time constants of 2,216 ± 190 ps and 305 ± 35 ps, respectively (Figure 6). There are still 21% of molecules remaining in the excited state a few ns after the excitation. In comparison, the Q-band GB for ZnPc at 675 nm has a major (70%) and a minor (30%) components with time constants of >5 ns and 283 ± 11 ps, respectively, and 28% molecules remain in the excited states 5 ns after the excitation (Figure 6). The major components of >5 ns in ZnPc and 2.2 ns in ZnHc are due to the S_1 state decay as seen in previous studies,[46,60] while the 300 ps component is due to the S_1 state decay in the aggregates as discussed below. Although the optical delay range limit prevents accurate determination of time constants longer than 2 ns, it is still a very good estimate that the singlet excited-state lifetime becomes shorter in ZnHc than in ZnPc by a factor of 2−3, while the quantum yield of intersystem crossing decreases by about 25%, measured by the remaining TA signals. The minor components with about 300 ps time constants are close to the singlet excited state decay time constant for covalently dimerized zinc phthalocyanine.[46]

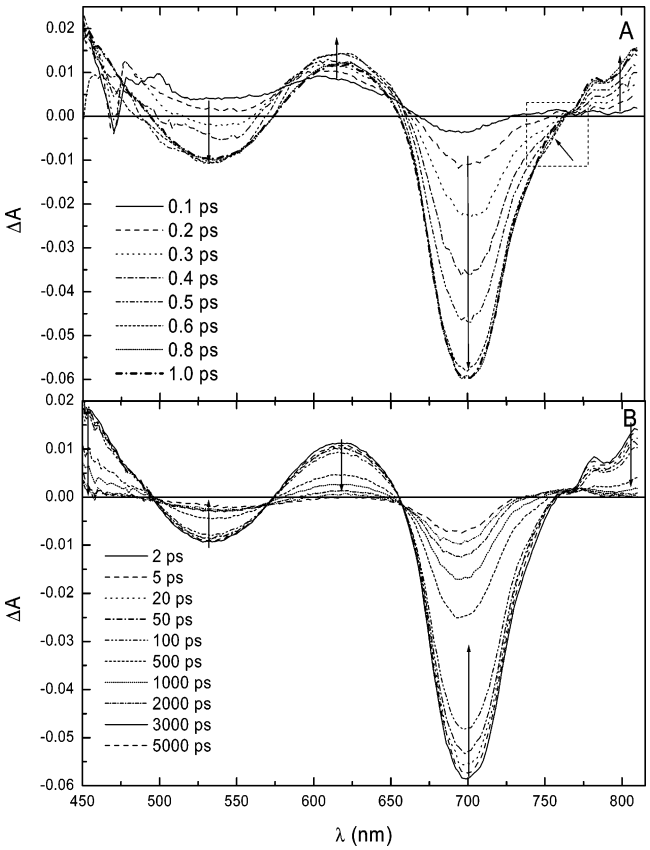

Figure 7. TA spectra of ZnHc in toluene with 410 nm light excitation and probe delays from 0.1 to 1 ps (A) and from 2 to 5000 ps (B).

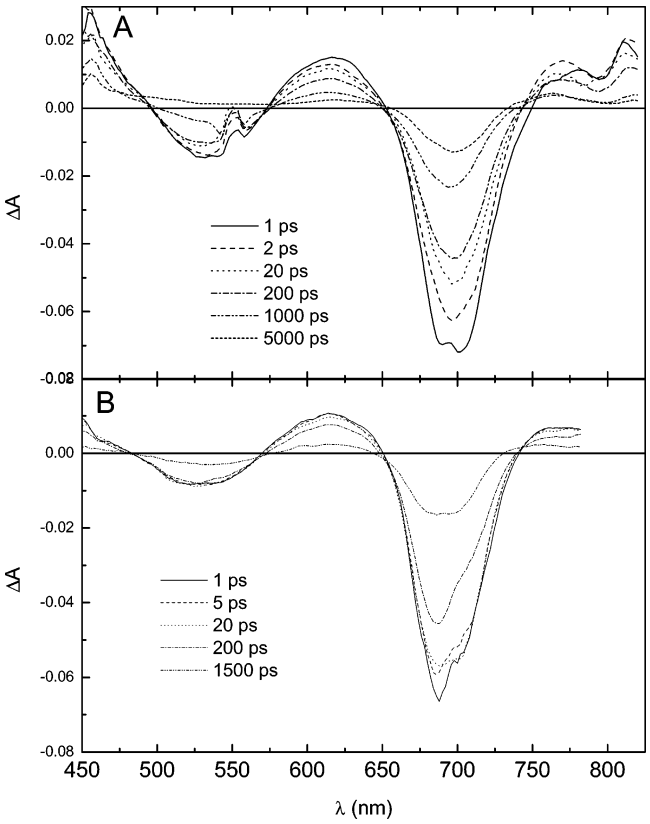

Figure 8. TA spectra of ZnHc in toluene with (A) 540 and (B) 690 nm light excitation and probe delays from 1 ps to over 1500 ps.

Self-Assembled ZnHc Aggregates. Exciting the self-assembled ZnHc dimer in toluene at the B-band, the broad 525 nm band and the Q-band respectively using 410, 540, and 690 nm light gives similar overall TA features (Figures 7 and 8) that drastically differ from those of the monomer. A new EA above the Q-band wavelength is observed for self-assembled ZnHc dimer, whereas no EA is observed for ZnHc monomer in the same region. Moreover, the appearance of the GB for the 525 nm broad band with the lower energy 690 nm excitation advocates for its origin as a new electronic transition due to self-assembly. Although there are only two GB regions for the Q-band and the 525 nm broad band respectively, the third GB region for the B band at 390 nm is below our detection limit. In addition, three EA regions of below 490 nm, 590−640 nm, and above 760 nm, respectively, are also observed (Figures 7 and 8). Main spectral features develop within 1 ps of the excitation, and still partially remain 5 ns after the excitation due to the triplet state.

Measured rate constants of excited state dynamics for self-assembled ZnHc in toluene are listed in Table 1, and kinetics traces under 410 nm excitation are depicted in Figure 9. When ZnHc is excited directly by the 690 nm light, the Q-band GB has an instantaneous bleaching, a recovery with 350 ps and a much longer time constant. The 350 ps time constant is independent of excitation wavelength and is associated with the singlet excited-state lifetime of self-assembled ZnHc dimer. When ZnHc is excited to a higher excited-state S_2 with 410 nm light, a 0.3 ps growth time constant is observed in the GB signal at 700 nm. This component could be due to a fast internal conversion of $S_2 \rightarrow S_0$. Additional fast GB recovery components are 650 fs when the B-band is excited and 4.9 ps when the 525 nm broad band is excited. The faster second time constant for the recovery, however, is excitation wavelength dependent, and is likely related to the internal conversion from S_2 to S_1, and from a new dimer excited-state X, induced by 540 nm excitation in the dimer, to S_0.

The unique GB centered at 525 nm is observed in the self-assembled dimeric ZnHc, and has instantaneous bleach followed by the apparent biexponential recovery with time constants of 510−556 ps and several ns. Only when the $S_0 \rightarrow S_2$ transition is induced by 410 nm light is an additional 300-fs recovery component observed. The appearance of the GB in this region with 690 nm light excitation indicates that the origin of the 525 nm broad band is not due to any impurity, but is corresponding to a new transition unique for self-assembled dimers. The consistently longer recovery/decay time constant of >500 ps compared to 350 ps for GB and EA at other probe wavelengths is due to spectral overlap between the EA of the singlet states and the GB of the broad 525 nm nm band. A simulation demonstrates that there is no clear distinction in terms of the goodness of the fit between two scenarios, two 350 ps components of opposite signs, and one 500 ps component.

The EA dynamics probed at 800 nm under the 410 nm nm excitation has the same time constants as that of the GB at 700 nm. The EA at ∼630 nm fits a triexponential function with time constants of 0.5−0.9 ps, 300−400 ps and much longer than a few ns under all three excitation wavelengths. In addition, a rise of the EA with about 300 fs time constant is observed only with 410 nm excitation, reflecting the internal conversion as mentioned above.

Compared to monomeric ZnHc, the singlet excited state lifetime of self-assembled ZnHc dimer is much shorter and the fraction of the long time component reflecting the inter-system crossing quantum yield is much lower. The self-assembly into dimeric aggregates causes the energy level splitting as well as the formation of a new state featured by the broad band at 525 nm. The increase of the density of states due to the self-

TABLE 1: Photoinduced Transient Kinetics of ZnHc in Toluene at 290 K

λ_{ex} (nm)	λ^{pro} (nm)	A^1 (%)	τ^1 (ps)	A^2 (%)	τ^2 (ps)	A_3[a] (%)	τ^3 (ps)	A_4[b] (%)
410	510	65	510 ± 25	10	0.3 ± 0.1			25
	618	58	388 ± 7	17	0.5 ± 0.2	rise	0.2 ± 0.02	25
	700	60	353 ± 5	15	0.65 ± 0.01	bleach	0.2 ± 0.02	25
	800	60	355 ± 10	25	0.68 ± 0.05	rise	0.3 ± 0.02	15
540	530	75	556 ± 20					25
	630	63	300 ± 4	21	0.6 ± 0.1			16
	690	60	339 ± 4	7	4.8 ± 1.2			33
690	530	73	546 ± 20					27
	630	80	400 ± 5	10	0.9 ± 0.1			10
	720	75	355 ± 4					25

[a] The fraction of the exponential component is not given because it counts for the growth of the signal. [b] This component is estimated by the remaining ΔA at the end of the scan, assuming the time constant is much longer than 4−5 ns.

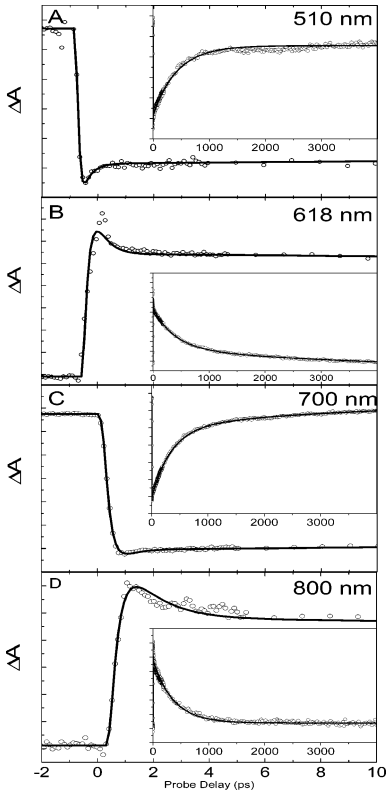

Figure 9. Room-temperature TA of ZnHc in toluene at different probe wavelengths (as labeled in each panel) as a function of probe delay time from the 410 nm pump pulse.

assembly opens additional routes for the excited state to return to the ground-state nonradiatively, which is evidenced by the quenching of the strong luminescence from a monomeric Q-band.

ZINDO/S Calculations for ZnPc and ZnHc Geometries Optimized at Different Levels of Theory. ZINDO/S calculations were performed for helicene, ZnPc, ZnHc monomer, and ZnHc dimer and trimer structures in order to determine changes in the optical spectra of the phthalocyanine influenced by functionalization and aggregation. Molecular geometries optimized at various levels of theory (PM3, HF/MINI-1*, HF/3-21G, B3LYP/3-21G, B3LYP/6-31G*) were used to analyze the sensitivity of the optical spectra to the level of approximation for structural optimization. The more accurate B3LYP geometry leads to the ZINDO/S Q-band of ZnPc at 745 nm, whereas the HF geometry gives 770 nm. Those are higher than the experimental value of 674 nm.[61] Both also produce the Soret band between 300 and 400 nm, similar to the experimental spectra. For comparison, ZnPc Q-band positions are 676 and 657 nm, respectively, from ZINDO/S calculations with 26/26 active orbitals at ZINDO and B88-PW91 geometries,[53] which is much closer to the experimental result than ours, but the B1/B2 band positions (293/283 nm using DFT geometry) are significantly lower than either experimental results (392/334 nm) or our calculations (347/324 nm). The discrepancy between the experiment and theory results from approximations made during geometry optimization and ZINDO parametrization. To facilitate a valid comparison to the experimental data, our calculations for ZnPc and ZnHc included eight $-OCH_3$ groups (to approximate eight $-OC_{12}H_{25}$ groups) attached to the Pc core for the former and to the helicenes for the latter, but such an approach leads only to small (i.e., 10 nm) changes in the transition energies. Although the more accurate B3LYP/6-31G* geometry from the B3LYP/6-31G* calculation significantly improves calculated results, it is too computationally demanding for larger ZnHc and its self-assembled aggregates. Also, the method does not include dispersion interaction which is believed to play a major role in self-assembly. Based on the comparison between several geometries of ZnHc obtained by different computational methods (Figure 10), we used everywhere geometries obtained at HF/MINI1* level complemented by dispersion terms, as described above.

Frontier Molecular Orbital (MO) Energy Levels. As shown by wave function distributions in Figure 11, the MOs of ZnHc have symmetry related counterparts to those of ZnPc, but they have the following differences: (a) the HOMO, LUMO+2 and LUMO+3 of ZnHc extend its wave function distribution beyond the Pc core; (b) HOMO-1, HOMO-2 and HOMO-3 are dominated by helicene wave functions, and (c) the symmetries of the wave function distribution for HOMO-1 and HOMO-4 are reversed with respect to aza N atoms. In ZnHc, wave functions of the Pc core only spread onto the first two C atoms beyond the benzo-ring shared by the Pc core and the helicene. Similar patterns of wave function distributions can be found in LUMO and LUMO+1. These two LUMOs are doubly degenerate in both ZnPc and ZnHc. It is evident that the HOMO and the LUMO of ZnHc are mostly localized on the Pc core and closely resemble those in the ZnPc. Hence, the MOs show evidence of limited π-conjugation between the core Pc and helicene side groups.

MO energy levels for helicene, ZnPc, ZnHc and its dimer are shown in Figure 12. Hybridization with helicene levels causes the LUMO of ZnHc to be lower than that of ZnPc leading to contraction of the HOMO−LUMO gap. This agrees with the observed red-shift of the Q-band of monomeric ZnHc relative to that of ZnPc because the main contribution of the Q-band is from the HOMO to LUMO transition.[53] The calculated optical absorption spectrum of ZnHc (Figure 12) shows a 12 nm red-shift of the Q-band relative to that of ZnPc as observed in the

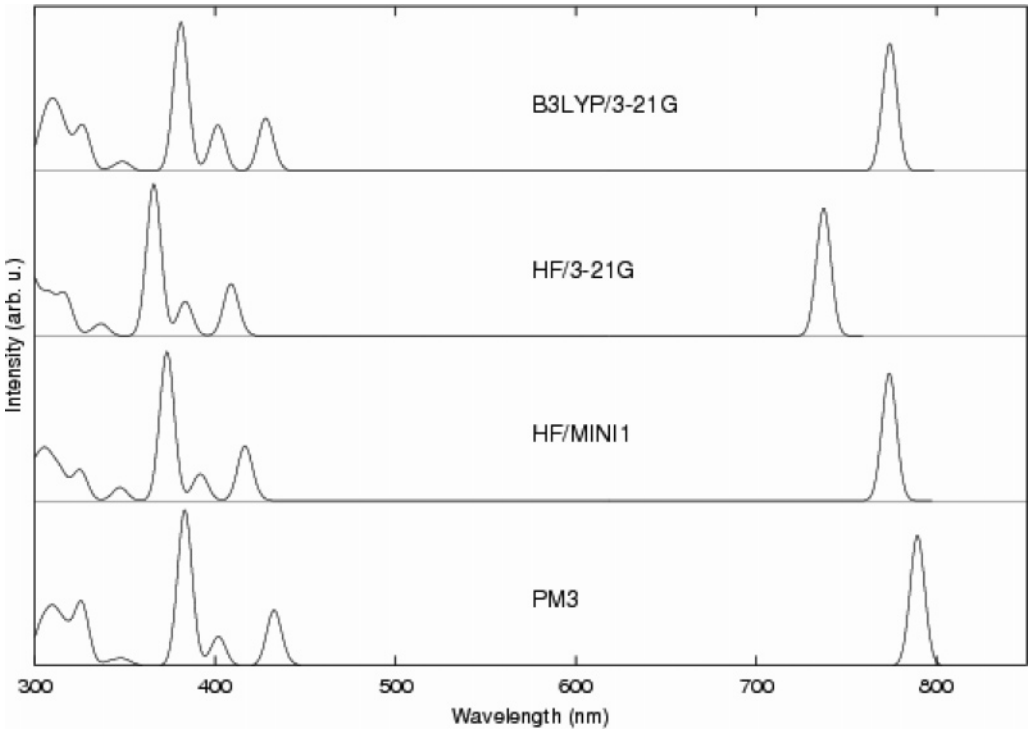

Figure 10. ZINDO/S spectra for ZnHc at different geometries.

experiment, although it is lower than experimental value of 75 nm. This transition has the same origin in ZnHc as in ZnPc.

Calculated Optical Absorption Spectra. Several occupied levels below HOMO of ZnHc are very different from those in ZnPc, because they are formed by the hybridization of helicene and Pc MOs (Figure 11). Transitions from these hybridized HOMO-1, HOMO-2, HOMO-3, and HOMO-4 levels to the LUMO produce a set of new transitions with lines at 422 and 416 nm in ZINDO/S spectra (Figures 12 and 13). In comparison, the lowest energy transitions of the B1 and B2 bands in ZnPc at 346 and 324 nm calculated using ZINDO/S are originated from completely localized HOMO-1 to the lower unoccupied orbitals. In the spectral region between the B- and the Q-bands, a calculated ZnPc transition at 375 nm with a small oscillator strength of 0.03 was attributed previously to the n$-\pi^*$ transition at 325 nm.[53] The new peaks at 422 and 416 nm for ZnHc are also red-shifted relative to the calculated helicene peak at 370 nm, which could correspond to the new shoulder in 400−500 nm region of the steady-state absorption spectrum (Figure 2), and is strongly red-shifted relative to both the ZnPc B-band and the lowest energy helicene absorption band.

The calculation also reproduced significant changes in the Q-band of ZnHc due to the dimer formation. Using the calculated geometry for the most stable dimer configuration, with one monomer being a mirror image rotated by 45° relative to the other, we have found that Q-band splits into a blue shifted band at 627 nm (HOMO, HOMO-1 to LUMO, LUMO+1 transition) and a band with a very low oscillator strength at 838 nm (Figure 13). This agrees with the exciton theory for H-aggregates where only the transition from the ground state to the higher exciton state is allowed. ZnHc trimer has a number of peaks with the HOMO−LUMO origin between 500 and 1000 nm, with the most prominent one at 589 nm. There are several weak bands in the 700−750 nm range as well. The trimer spectrum has striking resemblance with the experimental spectrum for the molecular aggregates in toluene (Figure 2), but will not agree with the results of SAXS data for the dimeric aggregates.

Discussion

Electronic Couplings between Zinc Phthalocyanine Core and Peripheral Helicenes. ZnHc has a unique structure among many peripherally substituted Pc derivatives, because the Pc core and the helicenes share the same benzo rings. The nonplanar helicenes prevent the π-electron delocalization over the entire ZnHc. On one hand, the ZnHc Q-band red-shifts by 1,402 cm^{-1} and its B-band, by 2528 cm^{-1}, relative to those of ZnPc, indicating an extended π-conjugation beyond the Pc core. This restricted π-conjugation is demonstrated by the electronic wave function distribution of frontier MOs (Figure 11), where the HOMO and LUMO of ZnHc have only small wave function contribution beyond the Pc core. On the basis of the four-level MO model for porphyrins and phthalocyanines, the Q-band and the B-band transitions are mainly from transitions of HOMO → LUMO and HOMO-1 → LUMO, respectively.[62] The decreases of the energy gaps for HOMO−LUMO and HOMO-1−LUMO in ZnHc compared to those of ZnPc agree qualitatively with the red-shifts of both Q- and B-bands of ZnHc relative to those of ZnPc (Figure 2). The red shift for the B-band is about twice of that for the Q-band, suggesting more significant influence of the helicene moieties on HOMO-1, HOMO-2, and HOMO-3. Therefore, more significant energy differences between the ZnPc and ZnHc appear among these HOMOs than those that appear among corresponding LUMOs. HOMO-1 and HOMO-2 of ZnHc have energies similar to the HOMO of helicene on the left (Figure 12) due to the hybridization of helicene dominant MOs with the Pc dominant MOs as the helicene fused with the Pc core. The spiral helicene forms the barrier for the π-electrons to delocalize. Under certain circumstances, different parts of the ZnHc may interact with other molecules or solvent independently, as discussed below.

Mechanism of Self-Assembly. ZnHc is constructed from helicene and Pc moieties, both of which self-assemble into one-dimensional aggregates at high concentrations or in certain solvents[24,49,59,63,64]. Interestingly, there is no evidence for large one-dimensional aggregates of ZnHc in solution even at a

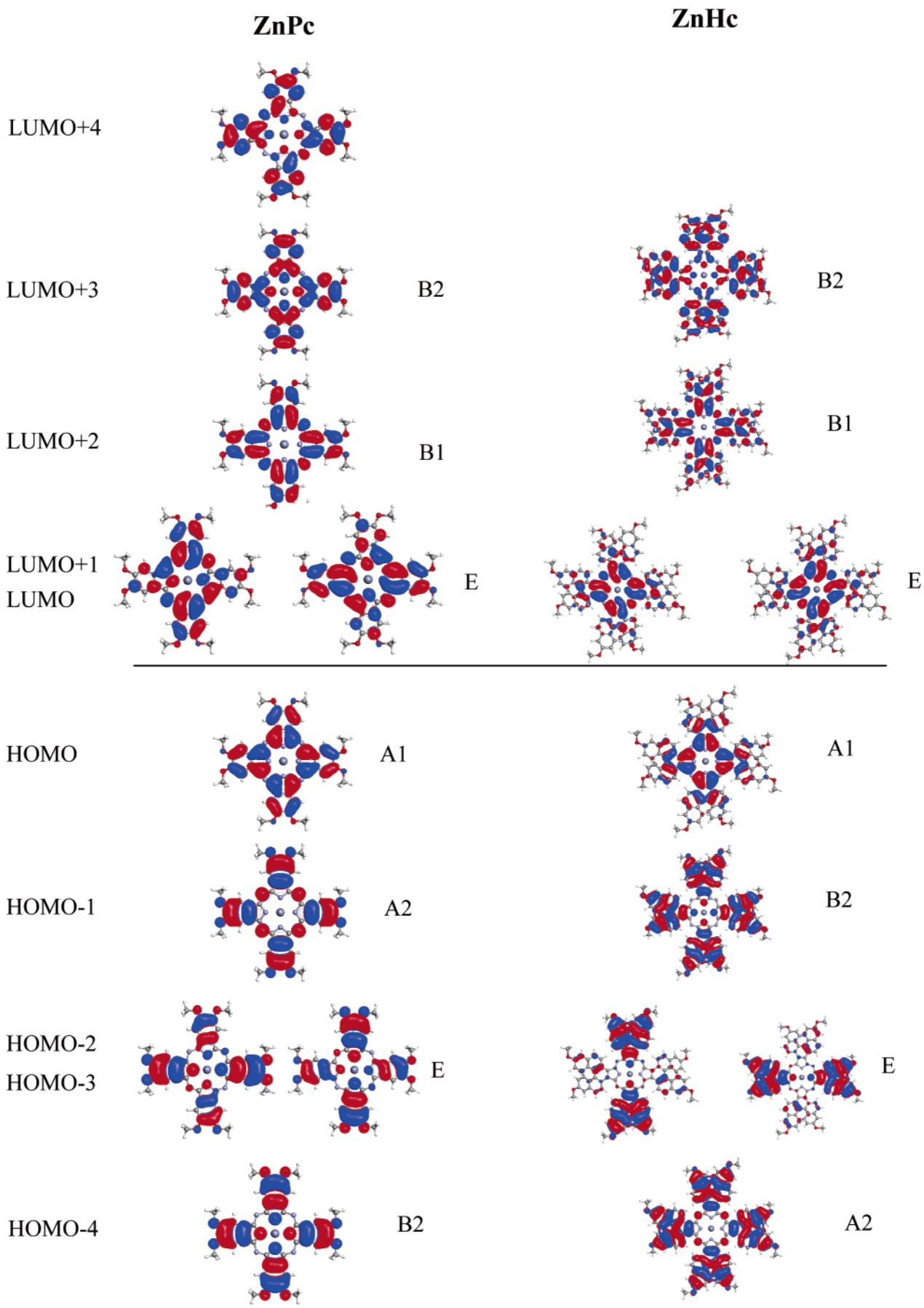

Figure 11. Frontier orbitals of monomeric ZnPc and ZnHc. Symmetry of the molecular orbitals is classified by irreducible representations of D4 point group.

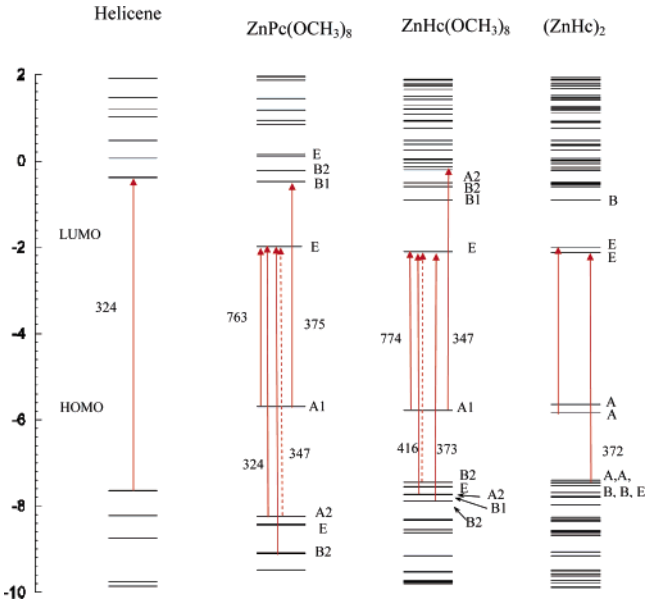

Figure 12. Partial molecular orbital diagram for helicene, ZnPc-(OCH3)$_8$, ZnHc, and ZnHc dimer. Orbital energies are calculated using ZINDO/S SCF. Orbital symmetries are in the notations of D4 group for ZnPc and ZnHc and in the notations of C4 for the ZnHc dimer. ZINDO/S transitions are indicated by arrows, where solid (dashed) lines are major (minor) components and the corresponding transition energies (in nm) are given next to the arrows.

concentration of $\sim 10^{-3}$ M (Figure 4), despite of its extraordinary capability of forming dimeric aggregates in solution. Therefore, it is import to analyze the origin for such a controlled self-assembly that was only known for covalent binding induced aggregation of Pc derivatives through metal ligation with peripheral crown ether groups[65] and by metal coordination through f-orbitals in sandwiched MPc_2 (M = metals with electrons in f orbitals, e.g., Lu).[66−68] In contrast, the self-assembly of ZnHc in solution involves only nonbonding interactions between neutral species. Reasons for the preference of ZnHc to the dimeric assemblies in a wide range of concentrations need to be analyzed by recognizing interplays between structural factors that either enhance or disrupt the self-assembly.

On one hand, $\pi-\pi$ interactions between helicene groups due to stacking is known to induce the formation of spiral fibrous filaments;[24,59] and $\pi-\pi$ interactions between Pcs make their stacking to form liquid crystals and films.[19,54,69] In a recent work, zinc phthalocyanine tetrakis(perylenediimide) showed enhanced self-assembly to form stacked aggregates with tens or even larger number of monomers.[70] Therefore, it is not surprising that ZnHc, with both core and peripheral of strongly $\pi-\pi$ interacting moieties, shows its extremely strong tendency of aggregation in solution. Moreover, our calculation shows that ZnHc has >99% population in either **1111** or **2222** conformation, which would minimize steric hindrance due to the entanglement between mismatched isomers in the dimer.

On the other hand, there are structural factors in ZnHc which may disrupt self-assembly. The vertical off-set between two ends of the helicene is about the same as the closest inter plane distance between two $\pi-\pi$ stacked Pcs, i.e., 3.3−3.6 Å. Therefore, the self-assembly of ZnHc can only be realized effectively when the nonplanar helicene from one ZnHc matches the spiral orientation of the helicene from the other, or when the stereo hindrance can be avoided by rotating one ZnHc relative to the other. Moreover, the eight long alkyloxy chains attached to each ZnHc have a tendency to randomly coil in solution with both gauche- and trans-conformations around each C−C bond. The flexible peripheral and the rigid core would have "virtual phase separation" with flexible alkyl chains wrapped around the core to prevent ZnHc to further stack as seen in the molecular dynamics simulation. Apparently, such a controlled self-assembly is unique for ZnHc, which does not occur in the smaller ZnPc or larger helicene fused Pcs with the same octa-dodecyloxy chains.[71]

Because of the interplay of these structural factors that exert opposite effects on self-assembly, ZnHc forms dimeric aggregates uniformly, which demonstrates the possibility of controlling molecular aggregates by balancing opposite effects on self-assembly through structural manipulation. It is important to select strongly interacting groups to promote self-assembly while attaching other accessory structures to disrupt the process. Obviously, the origin of the self-assembly and the capability of controlling such a process are of great interest for the design of molecular aggregates with desirable functions.

Self-Assembly Induced Electronic Interactions and Ultrafast Excited-State Dynamics. As described above, self-assembled ZnHc displays an optical absorption spectrum that covers almost the entire visible region with relatively high extinction coefficients, and optical responses that are mostly independent of the excitation wavelength. Such photophysical properties make the assembly a potential candidate for light harvesting and conversion. Hence, it is important to explore electronic structures and excited-state dynamics of the dimer as reflected by its unique optical properties, as well as their potential applications.

Changes in the Q- and B-bands in optical absorption of ZnHc due to the formation of the dimers in toluene, such as the blue-shift and the broadening, can be understood by the exciton theory approximation in molecular spectroscopy formulated by Kasha.[72] The approximation is based on interactions between transition dipoles, resulting in a splitting of two degenerate monomer states into two states with different energies, one higher and one lower in energy compared to the monomer state. In a face-to-face dimer, optical transitions from the ground state to the lower exciton state are symmetry-forbidden, while those to the higher exciton state are symmetry-allowed, resulting in a blue-shifted absorption.[72,73] In a head-to-tail dimer, the selection rule for the optical transition is reversed, resulting in a red-shifted absorption. The observed Q-band broadening for ZnHc in toluene happens mainly on the blue side of its corresponding monomeric Q-band at 746 nm, suggesting the formation of mostly H-aggregates from the stacking of the molecules.[73] The respectively blue-shifted peaks at 708 and 699 nm for ZnHc Q-band at 748 nm in toluene and hexane correspond to exciton splitting of 2674 and 2970 cm^{-1}. The solvent dependent blue-shift results from the variation of the dimer structures in different solvents other than the formation of larger aggregates, because only one peak besides the monomer Q-band can be identified. The larger blue-shift in hexane is an indication of stronger dipolar interactions than in toluene due to possibly closer distance between ZnHc monomers.

The most puzzling question is the origin of the 525 nm broad band in the absorption spectrum of the ZnHc dimer. This band is enhanced as a pronounced peak in the dimer spectrum while appears as a mere shoulder in the monomer spectrum. The shoulder feature has been observed in other alkoxy substituted Pcs, but very little explanation can be found in the literature. The only possible transition around 500 nm region was mentioned by Mack and Stillman as n → p* (n, nonbonding

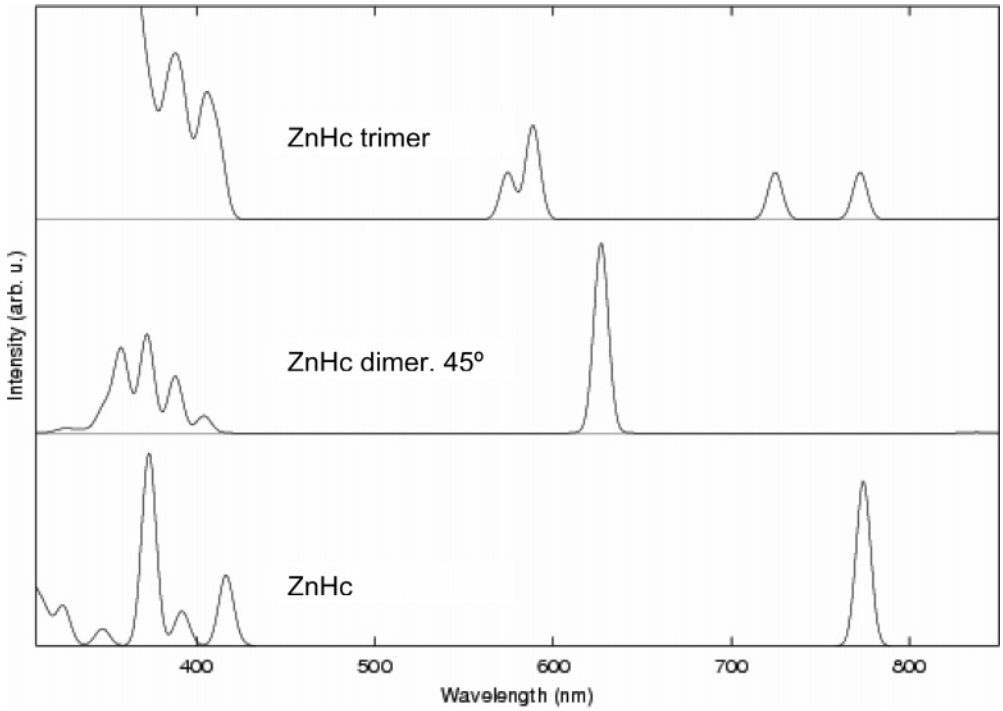

Figure 13. ZINDO/S optical spectra for (A) ZnHc monomer, (B) ZnHc dimer and (C) ZnHc trimer. Gaussian broadening is applied to the calculated discrete transitions for visualization.

orbital from the lone pair of aza N-atom) transitions with the z-polarization (out of the Pc plane).[53] The spiral structure of the fused helicene directly connected with alkoxy groups may promote coupling of localized MOs with the nonbonding lone pairs on O atom. The transition dipole could be further enhanced with the dimer formation because the *z*-polarized transition dipole can be further delocalized along the same direction between the two ZnHc molecules. Furthermore, the presence of the broad emission centered at 510 nm uniquely for the ZnHc dimer strongly supports its origin of the excimer emission due to interacting helicene groups for different ZnHc molecules through stacking (Figure 3). Similar spectral behavior due to the excimer emission of two adjacent perylene groups in a stacked zinc phthalocyanine tetrakis(perylenediimide) aggregate has been observed in a recent work.[70] The absence of such a transition in the 500 nm region in our ZINDO calculation is likely due to the deviation in the dimer structure, such as Zn−Zn distance, relative tilt and rotation angles between the monomers. The detailed exploration of the correlation between the structure and the absorption band position requires systematic variations of multiple structural parameters by large scale computations beyond the scope of this paper, which could be conducted in the future. The excited state dynamics measured by transient absorption in this region has no spectral features for the monomer ZnHc in OBCN, but has a distinct ground state bleaching band with slightly different kinetics compared to the Q-band independent of the excitation wavelength. Therefore, the origin of the 525 nm band is due to the self-assembly of ZnHc.

The excited-state lifetime of ZnHc monomer has been shortened by a factor of 2 −3 compared to ZnPc, which agrees with the prediction by the energy gap law[74] as the energy gap between S_0 and S_1 decreases from 1.83 to 1.66 eV. The excited-state lifetime for S_1 state for dimeric ZnHc is about 350 ps, about 10 times shorter than the monomer and comparable to and slightly longer than other dimeric Pcs.[46,60,75] Previous excited-state dynamics studies on Pc aggregates identified a decay/recovery component with a few to tens ps time constant that was attributed to the internal conversion from S_2 to S_1.[60] Our studies on ZnHc dimer only identified a fast component with subpicosecond time constants in addition to the 350 ps component for fitting most of the kinetic data. The subpicosecond component at 600−900 fs may be due to the internal conversion from the upper to the lower exciton states or possible sudden change in dimer conformation due to the shift of the electron density resulting from photoexcitation. Because a 200−300 fs growth time for both GB and EA signals only appears when S_2 state is excited and disappears when S_1 or the self-assembly induced new state is excited, its origin is likely due to the internal conversion from S_2 to other states. The faster internal conversion for ZnHc than for ZnPc[60] could be due to the existence of the dimerization induced new state that serves as additional pathways coupling S_2 and S_1 states. The precise assignments of these subpicosecond components are complicated due to spectral overlay from different intermediate species. However, effects of the π-conjugation expansion and the $\pi-\pi$ interaction through stacking on the excited-state dynamics are very clear as described above.

Conclusion

The most remarkable characteristics of ZnHc in solution is its capability of controlled self-assembly into uniform dimers in a wide range of concentrations (i.e., $10^{-3}-10^{-6}$M), resulting in an optical absorption spectrum with relatively high extinction coefficient in almost entire visible and near UV regions. Such a spectral coverage is mainly due to the rise of a new 525 nm broad band in the dimer spectrum, which can be explained by new electronic transitions with out-of-plane characters induced by the dimerization. The existence of the new state is only possible when the local intermolecular interactions are stronger or comparable with the intramolecular interactions in terms of π-conjugation and $\pi-\pi$ stacking. The continuous coverage of the entire spectral region is a desirable characteristic for harvesting solar energy, but quantum efficiencies for light energy conversion to charges, light and heat need to be explored further

by connecting ZnHc aggregates to molecular or other complex systems performing these functions.

Acknowledgment. The major funding of this work is sponsored by the Office of Basic Energy Sciences, U. S. Department of Energy under contract W-31-109-Eng-38. Use of the Advanced Photon Source was supported by the U. S. Department of Energy, Office of Science, Office of Basic Energy Sciences, under Contract W-31-109-Eng-38.

Supporting Information Available: Synthesis and spectroscopic data of ZnHc and Guinier plots for ZnHc in toluene. This material is available free of charge via the Internet at http://pubs.acs.org.

References and Notes

(1) Hanack, M.; Schneider, T.; Barthel, M.; Shirk, J. S.; Flom, S. R.; Pong, R. G. S. *Coord. Chem. Rev.* **2001**, *219*−*221*, 235.

(2) Nagamura, T. *Springer Ser. Photonics* **1999**, *2*, 376.

(3) Manas, E. S.; Spano, F. C.; Chen, L. X. *J. Chem. Phys.* **1997**, *107*, 707.

(4) Gregory, P. *J. Porphyrins Phthalocyanines* **2000**, *4*, 432.

(5) Kaliya, O. L.; Lukyanets, E. A.; Vorozhtsov, G. N. *J. Porphyrins Phthalocyanines* **1999**, *3*, 592.

(6) Zhou, H. S.; Honma, I. *Adv. Mater.* **1999**, *11*, 683.

(7) Costamagna, J.; Ferraudi, G.; Canales, J.; Vargas, J. *Coord. Chem. Rev.* **1996**, *148*, 221.

(8) Darwent, J. R.; Douglas, P.; Harriman, A.; Porter, G.; Richoux, M. C. *Coord. Chem. Rev.* **1982**, *44*, 83.

(9) Pandey, R. K. *CRC Handbook of Organic Photochemistry and Photobiology*, 2nd ed.; CRC Press: Boca Raton, FL, 2004; Vol. 144, p 1.

(10) Allen, C. M.; Sharman, W. M.; Van Lier, J. E. *J. Porphyrins Phthalocyanines* **2001**, *5*, 161.

(11) Schlettwein, D.; Jaeger, N. I.; Oekermann, T. Photoelectrochemical Reactions at Phthalocyanine Electrodes. In *Porphyrin Handbook*, 2003; Vol. 16, pp 247.

(12) Li, J.; Lindsey, J. S. *J. Org. Chem.* **1999**, *64*, 9101.

(13) Kobayashi, N. Synthesis and Spectroscopic Properties of Phthalocyanine Analogues. In *Porphyrin Handbook*; 2003; Vol. 15, pp 161.

(14) Rodriguez-Morgade, M. S.; De La Torre, G.; Torres, T. Design and Synthesis of Low-Symmetry Phthalocyanines and Related Systems. In *Porphyrin Handbook*; 2003; Vol. 15, pp 125.

(15) McKeown, N. B. The Synthesis of Symmetrical Phthalocyanines. In *Porphyrin Handbook*; 2003; Vol. 15, pp 61.

(16) Akutagawa, T.; Nakamura, T. *Springer Ser. Chem. Phys.* **2003**, *70*, 123.

(17) van de Craats, A. M.; Warman, J. M. *Adv. Mater.* **2001**, *13*, 130.

(18) Inabe, T. *J. Porphyrins Phthalocyanines* **2001**, *5*, 3.

(19) Van Nostrum, C. F. *Adv. Mater.* **1996**, *8*, 1027.

(20) Wada, T.; Hosoda, M.; Sasabe, H. *Adv. Chem. Ser.* **1994**, *240*, 303.

(21) Chen, L. X.; Mandal, B. K.; Bihari, B.; Sinha, A. K.; Kamath, M. *SPIE Proc.* **1995**, *2527*, 61.

(22) Mandal, B. K.; Bihari, B.; Sinha, A. K.; Kamath, M.; Chen, L. *Appl. Phys. Lett.* **1995**, *66*, 932.

(23) Tanaka, K.; Osuga, H.; Kitahara, Y. *J. Org. Chem.* **2002**, *67*, 1795.

(24) Nuckolls, C.; Katz, T. J.; Katz, G.; Collings, P. J.; Castellanos, L. *J. Am. Chem. Soc.* **1999**, *121*, 79.

(25) Nuckolls, C.; Katz, T. J.; Castellanos, L. *J. Am. Chem. Soc.* **1996**, *118*, 3767.

(26) Sooksimuang, T.; Behroozi, S. J.; Mandal, B. K. *J. Porphyrins Phthalocyanines* **2002**, *6*, 544.

(27) Greenfield, S. R.; Wasielewski, M. R. *Opt. Lett.* **1995**, *20*, 1394.

(28) Seifert, S.; Winans, R. E.; Tiede, D. M.; Thiyagarajan, P. *J. Appl. Cryst.* **2000**, *33*, 782.

(29) Tiede, D. M.; Zhang, R.; Seifert, S. *Biochemistry* **2002**, *41*, 6605.

(30) Svergun, D. I. General Theorems of Small-Angle Scattering by Disperse Systems. In *Neutron, X-ray and Light Scattering*; Lindner, P. Zemb, T. Eds.; North-Holland: Amsterdam, 1991; pp 83.

(31) Svergun, D. I. *Biophys. J.* **1999**, *76*, 2879.

(32) Stewart, J. J. P. *J. Comput. Chem.* **1989**, *10*, 209.

(33) Stewart, J. J. P. *J. Comput. Chem.* **1989**, *10*, 221.

(34) Hehre, W. J.; Radom, L.; Pople, J. A.; Schleyer, P. v. R. *Ab Initio Molecular Orbital Theory*; Wiley: New York, 1987.

(35) Tatewaki, H.; Sakai, Y.; Huzinaga, S. *J. Comput. Chem.* **1981**, *2*, 278.

(36) Kohn, W.; Becke, A. D.; Parr, R. G. *J. Phys. Chem.* **1996**, *100*, 12974.

(37) Ruan, C.-y.; Mastryukov, V.; Fink, M. *J. Chem. Phys.* **1999**, *111*, 3035.

(38) Tatewaki, H.; Huzinaga, S. *J. Comput. Chem.* **1980**, *1*, 205.

(39) Hobza, P.; Zahradnik, R. *Chem. Rev.* **1988**, *88*, 871.

(40) Elstner, M.; Hobza, P.; Frauenheim, T.; Suhai, S.; Kaxiras, E. *J. Chem. Phys.* **2001**, *114*, 5149.

(41) Curtiss, L. A.; Redfern, P. C.; Rassolov; Pople, J. A. Manuscript to be submitted.

(42) Thompson, M. A.; Zerner, M. C. *J. Am. Chem. Soc.* **1991**, *113*, 8210.

(43) Du, P.; Axe, F. U.; Loew, G. H.; Canuto, S.; Zerner, M. C. *J. Am. Chem. Soc.* **1991**, *113*, 8614.

(44) Leznoff, C. C., Lever, A. B. P., Eds. In *Phthalocyanines: Properties and Applications*; 1989.

(45) Ishii, K.; Kobayashi, N. The Photophysical Properties of Phthalocyanines and Related Compounds. In *Porphyrin Handbook*, 2003; Vol. 16; pp 1.

(46) Nikolaitchik, A. V.; Korth, O.; Rodgers, M. A. J. *J. Phys. Chem. A* **1999**, *103*, 7587.

(47) a) Kobayashi, N.; Mack, J.; Ishii, K.; Stillman, M. J. *Inorg. Chem.* **2002**, *41*, 5350. b) Konami, H.; Ikeda, Y.; Hatano, M.; *Mol. Phys.* **1993** *80*, 153−160.

(48) Fox, J. M.; Katz, T. J.; Van Elshocht, S.; Verbiest, T.; Kauranen, M.; Persoons, A.; Thongpanchang, T.; Krauss, T.; Brus, L. *J. Am. Chem. Soc.* **1999**, *121*, 3453.

(49) Kroon, J. M.; Koehorst, R. B. M.; van Dijk, M.; Sanders, G. M.; Sudholter, E. J. *J. Mat. Chem.* **1997**, *7*, 615.

(50) Bian, Y. Z.; Li, L.; Dou, J. M.; Cheng, D. Y. Y.; Li, R. J.; Ma, C. Q.; Ng, D. K. P.; Koboyashi, N.; Jian, J. Z. *Inorg. Chem.* **2004**, *43*, 7539.

(51) Stillman, M. J.; Nyokong, T. Absorption and Magnetic Circular Dichroism Spectral Properties of Phthalocyanines. In *Phthalocyanines: Properties and Applications*; Leznoff, C. C. Lever, A. B. P. Eds.; VCH Publishers, Inc.: New York, 1989; pp 202.

(52) Kobayashi, N. *Coord. Chem. Rev.* **2001**, *219*−*221*, 99.

(53) Mack, J.; Stillman, M. J. Electronic Structures of Metal Phthalocyanine and Porphyrin Complexes from Analysis of the UV−Visible Absorption and Magnetic Circular Dichroism Spectra and Molecular Orbital Calculations. In *Porphyrin Handbook*, 2003; Vol. 16, pp 43.

(54) Ban, K.; Nishizawa, K.; Ohta, K.; Shirai, H. *J. Mat. Chem.* **2000**, *10*, 1083.

(55) Kaneko, Y.; Nishimura, Y.; Takane, N.; Arai, T.; Sakuragi, H.; Kobayashi, N.; Matsunaga, D.; Pac, C.; Tokumaru, K. *J. Photochem. Photobiol. A: Chemistry* **1997**, *106*, 177.

(56) Chahraoui, D.; Valat, P.; Kossanyi, J. *Res. Chem. Intermed.* **1992**, *17*, 219.

(57) Fujitsuka, M.; Ito, O.; Konami, H. *Bull. Chem. Soc. Jpn.* **2001**, *74*, 1823.

(58) Gulbinas, V. *Chem. Phys.* **2000**, *261*, 469.

(59) Phillips, K. E. S.; Katz, T. J.; Jockusch, S.; Lovinger, A. J.; Turro, N. J. *J. Am. Chem. Soc.* **2001**, *123*, 11899.

(60) Howe, L.; Zhang, J. Z. *J. Phys. Chem. A* **1997**, *101*, 3207.

(61) Whalley, M. *J. Chem. Soc.* **1961**, 866.

(62) Gouterman, M. *J. Mol. Spectrosc.* **1972**, *44*, 37.

(63) Schutte, W. J.; Sluyters-Rehbach, M.; Sluyters, J. H. *J. Phys. Chem.* **1993**, *97*, 6069.

(64) Kimura, M.; Muto, T.; Takimoto, H.; Wada, K.; Ohta, K.; Hanabusa, K.; Shirai, H.; Kobayashi, N. *Langmuir* **2000**, *16*, 2078.

(65) Kobayashi, N.; Lever, A. B. P. *J. Am. Chem. Soc.* **1987**, *109*, 7433.

(66) Ishikawa, N.; Ohno, O.; Kaizu, Y. *J. Phys. Chem.* **1993**, *97*, 1004.

(67) Li, J.; Gryko, D.; Dabke, R. B.; Diers, J. R.; Bocian, D. F.; Kuhr, W. G.; Lindsey, J. S. *J. Org. Chem.* **2000**, *65*, 7379.

(68) Ishikawa, N. *J. Porphyrins Phthalocyanines* **2001**, *5*, 87.

(69) Kanezaki, E.; Yamanouchi, H.; Kanda, S. *Mol. Cryst. Liq. Cryst.* **1988**, *154*, 351.

(70) Li, X.; Sinks, L. E.; Rybtchinski, B.; Wasielewski, M. R. *J. Am. Chem. Soc.* **2004**, *126*, 10810

(71) Chen, L. X.; Shaw, G. B.; Tiede, D. M.; Zapol, P.; Redfern, P. C.; Curtiss, L. A.; Sooksimuang, T.; Mandal, B. K. Manuscript in preparation.

(72) Kasha, M.; Rawls, H. R.; El-Bayoumi, M. A. *Pure Appl. Chem.* **1965**, *11*, 371.

(73) McKeown, N. B. *Phthalocyanine Materials*; Cambridge University Press: Cambridge, 1998.

(74) Bixon, M.; Jortner, J.; Cortes, J.; Heitele, H.; Michel-Beyerle, M. E. *J. Phys. Chem.* **1994**, *98*, 7289.

(75) Gusev, A. V.; Danilov, E. O.; Rodgers, M. A. J. *J. Phys. Chem. A* **2002**, *106*, 1993.